

pubs.acs.org/JACS Communication

Voltammetric Detection of Singlet Oxygen Enabled by Nanogap Scanning Electrochemical Microscopy

Abhiroop Mishra, Michelle Zorigt, Dong Ok Kim, and Joaquín Rodríguez-López*



Cite This: J. Am. Chem. Soc. 2024, 146, 8847-8851



ACCESS I

Metrics & More

Article Recommendations

SI Supporting Information

ABSTRACT: Despite the significance of singlet oxygen $(^{1}O_{2})$ in several biological, chemical, and energy storage systems, its voltammetric reduction at an electrode remains unreported. We address this issue using nanogap scanning electrochemical microscopy (SECM) in substrate-generation/tip-collection mode. Our investigation reveals a reductive process on the SECM tip at -1.0 V (vs Fc⁺/Fc) during the breakdown of the $\text{Li}_{2}\text{CO}_{3}$ substrate in deuterated acetonitrile. Notably, this value is approximately 0.9 V more positive than the reduction potential of triplet oxygen ($^{3}\text{O}_{2}$), consistent with thermodynamic estimates for the energy of the formation of $^{1}\text{O}_{2}$. This finding holds significant implications for understanding the reaction mechanisms involving $^{1}\text{O}_{2}$ in nonaqueous media.

T he excited states of molecular dioxygen, known as singlet oxygen, were first identified in 1924 and have since been extensively studied in biological and chemical systems. $^{1-4}$ The two excited singlet states differ from the triplet ground state $(^3\mathrm{O}_2)$ in their electronic structure, particularly in the π -antibonding orbitals causing differences in their multiplicity. 2 The lowest energy singlet state, $^1\mathrm{O}_2$ (or $^1\Delta_g$), has found several applications, ranging from photodynamic therapy for cancer to organic synthesis of molecules. 5,6 More recently, there has been an immense interest in the role of $^1\mathrm{O}_2$ in the degradation of advanced electrochemical energy storage systems, such as Li-ion and metal—air batteries. $^{7-15}$

The formation energy of ¹O₂ is 95 kJ/mol higher than the ³O₂ state, attributed to the presence of antiparallel electron spins in the π -antibonding orbital.² This imparts ${}^{1}O_{2}$ with highly oxidizing properties, thereby classifying it as a reactive oxygen species (ROS). Dissolved in liquid media, ¹O₂ lasts only a few microseconds before undergoing spontaneous deactivation processes, converting to the more stable ³O₂ state. 16,17 These deactivation pathways primarily include energy transfer to solvent vibrational levels, phosphorescent radiation emission at 1270 nm (which distinguishes it from ³O₂), and reactions with other species.² The lifetime of ¹O₂ in water is just 3.5 μ s,¹⁷ thus presenting challenges to its experimental investigation. Nonetheless, researchers have made significant strides in characterizing its physical and chemical properties over the past few decades.² Typical ¹O₂ detection methods involve monitoring these photon emissions during its decay to 3O2 or using chemical spin traps that undergo structural changes upon exposure to ${}^{1}\!O_{2}$. 18,19

Given the widespread presence of ${}^{1}O_{2}$ in various chemical, biological, and electrochemical systems, determining its electrochemical properties simultaneously addresses a fundamental question while providing a deeper insight into its reactivity. While the direct electrochemical detection of ${}^{3}O_{2}$ is commonplace, ${}^{20-22}$ to our knowledge, it has never been reported for ${}^{1}O_{2}$. The IUPAC technical report lists the

standard reduction potential (E^0) of ${}^1O_{22}^{23}$ however, it has never been experimentally characterized at an electrode. The E^0 , notably 0.99 V more positive than that of 3O_2 for a one-electron-reduction process, underscores the urgent need for experimental characterization of this species to better characterize its reactivity and generation.

In this work, nanogap scanning electrochemical microscopy (SECM) was employed for the experimental characterization of the reduction potential of $^{1}O_{2}$ in nonaqueous media. The electrochemical oxidation of $\text{Li}_{2}\text{CO}_{3}$, which has been reported as a highly selective source for $^{1}O_{2}$, served as an in situ source of this elusive species. SECM allowed us to position a Ptnanoelectrode close to $\text{Li}_{2}\text{CO}_{3}$ substrate in a deuterated acetonitrile (D-MeCN) solution, where a higher lifetime of the species is reported. This proximity facilitated a very high temporal resolution of the measurement (\sim 80 μ s) and enabled the electrochemical reduction of $^{1}O_{2}$. Our findings revealed a substantial 0.9 V difference between the reduction potential of $^{1}O_{2}$ and that of $^{3}O_{2}$, corroborating well with the IUPAC report. 23

Figure S1 shows the schematic of the SECM cell used in this study. It features a four-electrode configuration, including a Pt/polypyrrole reference electrode²⁶ and a Pt counter electrode. The working electrodes consist of a 300 nm radius Pt-nanoelectrode and a Li₂CO₃ substrate. In 2018, Freunberger and colleagues reported that electrochemical oxidation of Li₂CO₃ produces ¹O₂. ²⁴ They used 9,10-dimethylanthracene as a selective chemical spin trap to confirm ¹O₂ generation and ensured stability against other reactive oxygen species. ¹³

Received: January 10, 2024 Revised: March 15, 2024 Accepted: March 18, 2024 Published: March 21, 2024





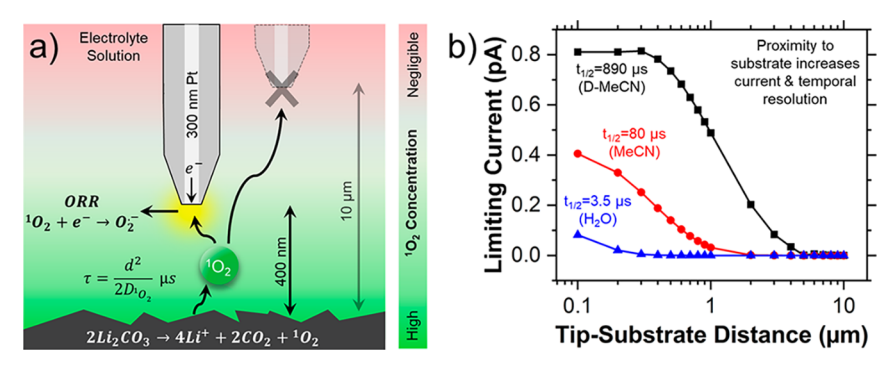


Figure 1. a) Illustration of the processes occurring at the electrode–electrolyte interface during SECM measurement. D_{0} represents the diffusion coefficient of ${}^{1}O_{2}$ and τ represents its diffusion time over distance (d). b) COMSOL simulations showing the mass transfer limited current for ${}^{1}O_{2}$ reduction at 300 nm Pt-nanoelectrode in different solvents as a function of tip–substrate distance, assuming the flux of ${}^{1}O_{2}$ from the substrate as 5 \times 10⁻⁶ mol/m²s (\sim 0.5 A/m²). $t_{1/2}$ refers to the half-life of ${}^{1}O_{2}$.

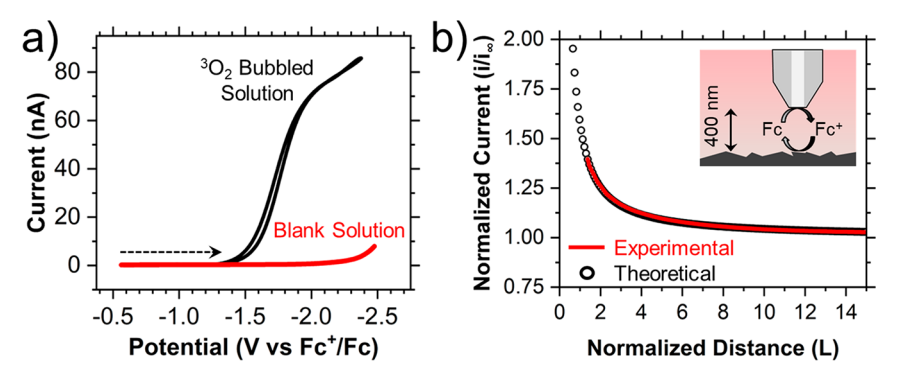


Figure 2. a) Cyclic voltammograms under an Ar atmosphere (red) and after bubbling the solution with ${}^{3}O_{2}$ (black). b) SECM approach curve to position the Pt-nanoelectrode approximately 400 nm away from the $Li_{2}CO_{3}$ substrate. Ferrocene served as the redox mediator during the approach curves.

Online electrochemical mass spectrometry further validated the absence of any 3O_2 during the process. 24 Furthermore, researchers have since employed DFT calculations to elucidate on the kinetic driving force for the selective formation of 1O_2 during this Li_2CO_3 oxidation, 27 thereby making it an ideal choice as the substrate in this work. Further details about the SECM substrate preparation can be found in the Supporting Information along with the SEM micrographs (Figure S2).

Figure 1a illustrates the SECM measurement. An oxidizing potential applied to the Li₂CO₃ facilitates its breakdown and consequent release of 1 O₂. 24,25 1 O₂ is intercepted by the SECM tip, which is biased at a potential to enable its reduction before it decays. Figure 1b shows the simulated response for our setup and experimental parameters, showcasing its dependence on the tip—substrate distance and the reported lifetime in different solvents. 17 Increasing the tip—substrate distance extends the diffusional time (τ) and thus intercepts a lower concentration of 1 O₂, resulting in lower currents. Consequently, our process requires two key elements: 1) the precise positioning of the Ptnanoelectrode near the Li₂CO₃ substrate to detect 1 O₂, and 2) biasing of the nanoelectrode to a potential that selectively reduces 1 O₂ while avoiding the other species released during Li₂CO₃ breakdown, such as CO₂, 3 O₂, and Li⁺. 24,25

SECM was uniquely positioned to tackle the first challenge. The use of a robust 300 nm radius Pt-nanoelectrode²⁸ allowed us to position it in a straightforward manner \sim 400 nm from the substrate, resulting in an approximately 80 μ s temporal resolution for the measurement. Nanoelectrodes possess a significantly higher mass transfer coefficient compared to

larger-sized electrodes.²⁹ This is particularly advantageous for capturing transient species with short lifetimes. 30,31 Furthermore, D-MeCN was used as the solvent in the SECM measurements. Differences in 1O2 lifetime among solvents result from varying energy transfer efficiencies from the electronic states of ¹O₂ to vibrational states of solvent. ^{16,17} In solvents such as water, not only is the lifetime of ¹O₂ too short $(3.5 \mu s)$, 17 but the electrochemical detection would be hampered by the electrochemical oxidation of water and of the electrode surface if the reduction of ¹O₂ occurred ~0.99 V more positive than that of 3O_2 . ²³ In D-MeCN, the lifetime of $^{1}O_{2}$ is 890 μ s, 17 thereby increasing the chances of detecting it before it decays. Furthermore, SECM offers the advantage of using a Li₂CO₃ substrate, which generates ¹O₂ without requiring the presence of ³O₂ in the solution as it is typically done in photosensitizer-mediated approaches.^{24,27} This facilitates the unambiguous electrochemical characterization of the ¹O₂ reduction potential.

To identify the potential window to be applied at the Ptnanoelectrode during SECM measurements, we first characterized the reduction potential of $^3\mathrm{O}_2$ in D-MeCN. All potentials in this communication are referenced versus the ferrocene redox couple. Cyclic voltammograms in Figure 2a were obtained at a 12.5 μ m radius Pt working electrode in 0.1 M TBAPF₆ D-MeCN under two conditions. The red voltammogram, recorded in an Ar-filled glovebox (with O_2 and $\mathrm{H}_2\mathrm{O}$ less than 0.1 ppm), showed no discernible Faradaic process. However, when $^3\mathrm{O}_2$ was bubbled into the solution, a clear peak corresponding to its reduction emerged beyond

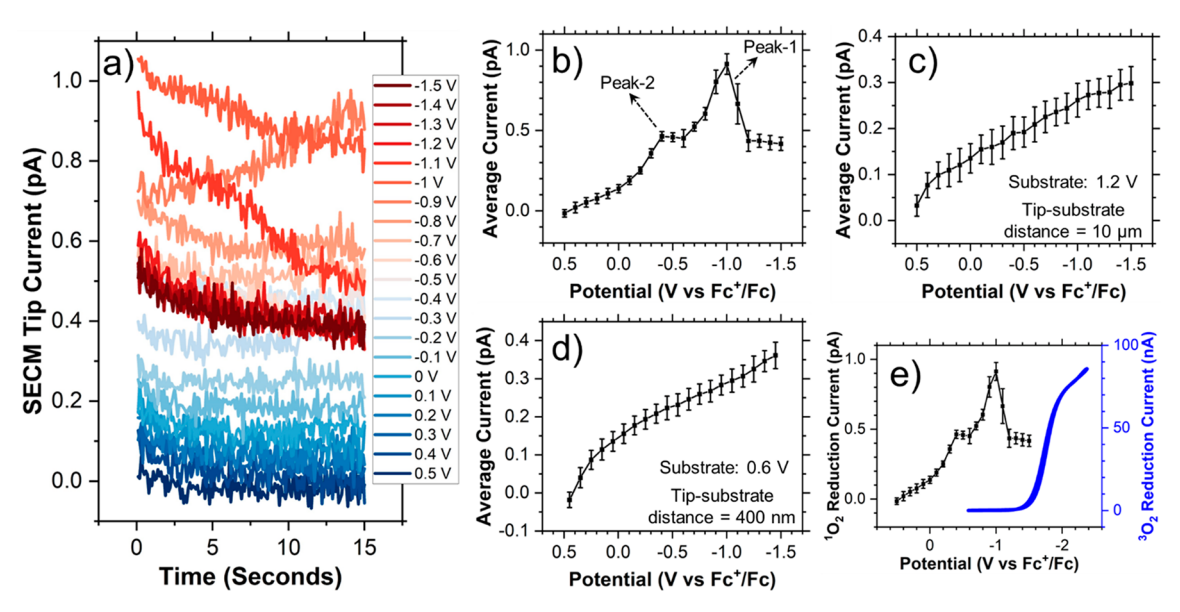


Figure 3. a) Current—time response at the Pt-nanoelectrode at different potentials. Average current as a function of potential at b) 400 nm and c) $10 \mu m$ tip—substrate distance, respectively; d) 400 nm tip—substrate distance, substrate biased at 0.6 V. The error bars correspond to the standard deviation of the 15 s current response at the SECM tip for each specific potential. e) Electrochemical reduction response of $^{1}O_{2}$ and $^{3}O_{2}$ in D-MeCN.

-1.5 V, as seen in the black curve. Theoretically, the standard reduction potential of $^{1}O_{2}$ should be more positive than that of $^{3}O_{2}$. This information guided us to limit the potential window for SECM experiments to values more positive than -1.5 V for avoiding interference from $^{3}O_{2}$ reduction

The SECM measurement began by precisely positioning the Pt nanoelectrode ~400 nm from the Li₂CO₃ substrate. This was done via approach curves using ferrocene as a redox mediator, as illustrated in Figure 2b. 32 The ferrocene solution was then carefully rinsed and replaced with 0.1 M TBAPF₆ D-MeCN. Additional details on approach curves and the cell rinsing procedure are available in the Supporting Information, Figure S3. The nanoelectrode was then biased with a staircase waveform from 0.5 to -1.5 V in 0.1 V decrements, each held for 15 s (Figure S4). The substrate was maintained at 1.2 V throughout the 315 s experiment, which facilitated electrochemical oxidation of Li₂CO₃, releasing ¹O₂ in the process, which then diffuses to the nanoelectrode. 24,25 The nanoelectrode potential ranged from 0.5 to -1.5 V, with the anticipation that a higher current would be recorded at the potentials associated with reduction of ${}^{1}O_{2}$.

Figure 3a displays the current-time response overlay for various potentials applied to the nanoelectrode during the SECM experiment. Qualitatively, higher currents were observed around −1 V as shown in Figure 3a. For a more comprehensive analysis, we calculated the average current over the 15 s duration at each potential and plotted it as a function of nanoelectrode potential in Figure 3b. At -1 V, a prominent peak emerged (peak-1), while at -0.5 V, a smaller yet discernible peak was evident (peak-2). Peak-1 is approximately 0.9 V more positive than the potential of ³O₂ reduction (Figure 2a), strongly suggesting that it corresponds to the reduction of the ¹O₂ species. Possible reasons for the peak-shaped response are explained in Figure S5, but one key possibility is a decreasing substrate current. Furthermore, the substrate current (~2 A/m2 at the peak) should translate to a tip response of \sim 3 pA (Figure S5f); however, we observed \sim 1 pA. We posit that such a decrease is explained by a following chemical step where the tip-generated superoxide radical anion $(O_2^{\bullet-})$ may exchange with 1O_2 in the diffusion layer, reforming $O_2^{\bullet-}$ but producing 3O_2 . 3O_2 is not reducible at the tip potential, and thus inactive, causing a decrease in the measured current, Figure S5g. It is worth noting that peak-1 is reproducible and remains consistent across different SECM measurements on fresh Li_2CO_3 substrates, as shown in Figure S6. Minor variations in the peak current in these trials can be attributed to the heterogeneity of the Li_2CO_3 substrate. Detailed COMSOL simulations illustrating this point are available in Figure S7. On the other hand, peak-2 lacked reproducibility in different SECM measurements. It was observed in only 2 of 10 independent control experiments (Figure S8) in a Li^+ electrolyte with 3O_2 , suggesting it as a process unrelated to 1O_2 .

To validate our association of peak-1 with $^1\mathrm{O}_2$ reduction, we performed additional control experiments. First, given the transient nature of $^1\mathrm{O}_2$, we demonstrated that a sufficiently large tip—substrate distance results in the loss of the cathodic feature at the nanoelectrode, as evident in Figure 3c, where the Pt-nanoelectrode was $10~\mu\mathrm{m}$ away from the substrate. Second, we conducted a measurement with a 400 nm tip—substrate distance, where the substrate was biased at a potential insufficient to trigger $\mathrm{Li_2CO_3}$ breakdown and subsequent $^1\mathrm{O}_2$ release. The absence of peak-1 in this case, as shown in Figure 3d, reinforces our assertion regarding its correlation with $^1\mathrm{O}_2$ reduction.

We next validated the selectivity of our SECM method toward 1O_2 and eliminated the possibility of peak-1 being attributed to D-MeCN breakdown. This was accomplished by utilizing a glassy carbon electrode as the substrate during SECM measurement, i.e., in the absence of Li_2CO_3 , using the same parameters as in Figure 3a. Once again, no peak was observed (Figure S9). Finally, we studied the effect of CO_2 and Li^+ , released in addition to 1O_2 during electrochemical oxidation of Li_2CO_3 . Control experiments, as depicted in Figure S10, confirmed the electrochemical inactivity of CO_2 and Li^+ within the potential window of interest. This eliminates

the possibility of their affecting the nanoelectrode response. It is important to note that peak-1 was seen exclusively in D-MeCN solvent and was not present in MeCN (Figure S11), where the $^{1}\text{O}_{2}$ lifetime is approximately 60 μ s. ¹⁷ Simulations (Figure 1b) indicate the nanoelectrode must be positioned less than 100 nm from the substrate to record appreciable current, a challenging task for nonatomically flat substrate.

It should be noted that the ${}^3{\rm O}_2$ reduction potential is influenced by the nature of the cations in solution. However, pioneering work by K. M. Abraham and colleagues suggests that, depending upon the cation identity, the difference is limited to $\sim 0.2~{\rm V.}^{33,34}$ Therefore, despite the additional presence of Li⁺ in the nanoelectrode's vicinity due to the breakdown of Li₂CO₃, we dismiss the possibility that peak-1 corresponds to the shifted reduction response of ${}^3{\rm O}_2$. Therefore, through the set of above-mentioned control experiments, we rule out additional possibilities and confidently assign peak-1 to the reduction of ${}^1{\rm O}_2$. In Figure 3e, the electrochemical reduction responses of ${}^1{\rm O}_2$ and ${}^3{\rm O}_2$ are compared, experimentally highlighting their significant difference—a fact previously known only theoretically.²³

In conclusion, this study was designed to address a fundamental gap in our knowledge of $^{1}O_{2}$ species by experimentally characterizing its electrochemical reduction potential, which we set at -1 V in D-MeCN. This work holds substantial implications for the comprehension of reaction mechanisms involving $^{1}O_{2}$, including metal—air- and transition-metal-oxide-based alkali ion batteries in nonaqueous media.

ASSOCIATED CONTENT

Supporting Information

The Supporting Information is available free of charge at https://pubs.acs.org/doi/10.1021/jacs.4c00414.

Further details of the experimental and simulation procedures such as scanning electrochemical microscopy measurements, scanning electron microscopy images, and COMSOL multiphysics simulations (PDF)

AUTHOR INFORMATION

Corresponding Author

Joaquín Rodríguez-López — Department of Chemistry, University of Illinois Urbana—Champaign, Urbana, Illinois 61801, United States; orcid.org/0000-0003-4346-4668; Phone: 217-300-7354; Email: joaquinr@illinois.edu

Authors

Abhiroop Mishra — Department of Chemistry, University of Illinois Urbana—Champaign, Urbana, Illinois 61801, United States; © orcid.org/0000-0003-3403-4455

Michelle Zorigt — Department of Chemistry, University of Illinois Urbana—Champaign, Urbana, Illinois 61801, United States; © orcid.org/0000-0001-6764-5995

Dong Ok Kim – Department of Chemistry, University of Illinois Urbana–Champaign, Urbana, Illinois 61801, United States; Occid.org/0009-0000-0539-5767

Complete contact information is available at: https://pubs.acs.org/10.1021/jacs.4c00414

Notes

The authors declare no competing financial interest.

ACKNOWLEDGMENTS

The authors acknowledge financial support from the National Science Foundation under CHE Grant 2004054. A.M. gratefully acknowledges the support from the Link Foundation Energy Fellowship. We thank Peisen Qian for valuable discussions. Sample preparation and characterization were carried out in part in the Materials Research Laboratory at the University of Illinois.

REFERENCES

- (1) Stuhr, R.; Bayer, P.; von Wangelin, A. J. The Diverse Modes of Oxygen Reactivity in Life & Chemistry. *ChemSusChem* **2022**, *15* (24), No. e202201323.
- (2) Wang, Y.; Lin, Y.; He, S.; Wu, S.; Yang, C. Singlet oxygen: Properties, generation, detection, and environmental applications. *J. Hazard. Mater.* **2024**, *461*, No. 132538.
- (3) Herzberg, G. Photography of the Infra-Red Solar Spectrum to Wave-length 12,900 A. *Nature* **1934**, *133* (3368), 759–759.
- (4) Xie, Z.-H.; He, C.-S.; Pei, D.-N.; Dong, Y.; Yang, S.-R.; Xiong, Z.; Zhou, P.; Pan, Z.-C.; Yao, G.; Lai, B. Review of characteristics, generation pathways and detection methods of singlet oxygen generated in advanced oxidation processes (AOPs). *Chem. Eng. J.* **2023**, *468*, No. 143778.
- (5) Ghogare, A. A.; Greer, A. Using Singlet Oxygen to Synthesize Natural Products and Drugs. *Chem. Rev.* **2016**, *116* (17), 9994–10034.
- (6) Maharjan, P. S.; Bhattarai, H. K. Singlet Oxygen, Photodynamic Therapy, and Mechanisms of Cancer Cell Death. *J. Oncol.* **2022**, 2022, No. 7211485.
- (7) Schürmann, A.; Luerßen, B.; Mollenhauer, D.; Janek, J.; Schröder, D. Singlet Oxygen in Electrochemical Cells: A Critical Review of Literature and Theory. *Chem. Rev.* **2021**, *121* (20), 12445—12464.
- (8) Mahne, N.; Schafzahl, B.; Leypold, C.; Leypold, M.; Grumm, S.; Leitgeb, A.; Strohmeier, G. A.; Wilkening, M.; Fontaine, O.; Kramer, D.; Slugovc, C.; Borisov, S. M.; Freunberger, S. A. Singlet oxygen generation as a major cause for parasitic reactions during cycling of aprotic lithium—oxygen batteries. *Nat. Energy* **2017**, *2* (5), No. 17036.
- (9) Schafzahl, L.; Mahne, N.; Schafzahl, B.; Wilkening, M.; Slugovc, C.; Borisov, S. M.; Freunberger, S. A. Singlet Oxygen during Cycling of the Aprotic Sodium—O₂ Battery. *Angew. Chem., Int. Ed.* **2017**, *56* (49), 15728—15732.
- (10) Petit, Y. K.; Mourad, E.; Prehal, C.; Leypold, C.; Windischbacher, A.; Mijailovic, D.; Slugovc, C.; Borisov, S. M.; Zojer, E.; Brutti, S.; Fontaine, O.; Freunberger, S. A. Mechanism of mediated alkali peroxide oxidation and triplet versus singlet oxygen formation. *Nat. Chem.* **2021**, *13* (5), 465–471.
- (11) Wandt, J.; Freiberg, A. T. S.; Ogrodnik, A.; Gasteiger, H. A. Singlet oxygen evolution from layered transition metal oxide cathode materials and its implications for lithium-ion batteries. *Mater. Today* **2018**, *21* (8), 825–833.
- (12) Genreith-Schriever, A. R.; Banerjee, H.; Menon, A. S.; Bassey, E. N.; Piper, L. F. J.; Grey, C. P.; Morris, A. J. Oxygen hole formation controls stability in LiNiO₂ cathodes. *Joule* **2023**, *7* (7), 1623–1640.
- (13) Mondal, S.; Jethwa, R. B.; Pant, B.; Hauschild, R.; Freunberger, S. A. Singlet oxygen formation in non-aqueous oxygen redox chemistry: direct spectroscopic evidence for formation pathways and reliability of chemical probes. *Faraday Discuss.* **2024**, 248, 175–189.
- (14) Ahn, S.; Zor, C.; Yang, S.; Lagnoni, M.; Dewar, D.; Nimmo, T.; Chau, C.; Jenkins, M.; Kibler, A. J.; Pateman, A.; Rees, G. J.; Gao, X.; Adamson, P.; Grobert, N.; Bertei, A.; Johnson, L. R.; Bruce, P. G. Why charging Li—air batteries with current low-voltage mediators is slow and singlet oxygen does not explain degradation. *Nat. Chem.* **2023**, *15* (7), 1022–1029.
- (15) Dong, S.; Yang, S.; Chen, Y.; Kuss, C.; Cui, G.; Johnson, L. R.; Gao, X.; Bruce, P. G. Singlet oxygen and dioxygen bond cleavage in the aprotic lithium-oxygen battery. *Joule* **2022**, *6* (1), 185–192.

- (16) Thorning, F.; Henke, P.; Ogilby, P. R. Perturbed and Activated Decay: The Lifetime of Singlet Oxygen in Liquid Organic Solvents. *J. Am. Chem. Soc.* **2022**, *144* (24), 10902–10911.
- (17) Bregnhøj, M.; Westberg, M.; Jensen, F.; Ogilby, P. R. Solvent-dependent singlet oxygen lifetimes: temperature effects implicate tunneling and charge-transfer interactions. *Phys. Chem. Chem. Phys.* **2016**, *18* (33), 22946–22961.
- (18) You, Y. Chemical tools for the generation and detection of singlet oxygen. Org. Biomol. Chem. 2018, 16 (22), 4044–4060.
- (19) Zhou, Y.; Dong, J.; Zhao, Y.; Mao, Z. Singlet Oxygen Generation via an Electrochemical Reduction Method Assisted by a Ruthenium(II) Complex. *Inorg. Chem.* **2023**, *62* (19), 7155–7159.
- (20) Schwager, P.; Fenske, D.; Wittstock, G. Scanning electrochemical microscopy of oxygen permeation through air-electrodes in lithium—air batteries. *J. Electroanal. Chem.* **2015**, 740, 82—87.
- (21) Mishra, A.; Sarbapalli, D.; Hossain, M. S.; Gossage, Z. T.; Li, Z.; Urban, A.; Rodríguez-López, J. Highly Sensitive Detection and Mapping of Incipient and Steady-State Oxygen Evolution from Operating Li-Ion Battery Cathodes via Scanning Electrochemical Microscopy. J. Electrochem. Soc. 2022, 169 (8), No. 086501.
- (22) Dobrzeniecka, A.; Zeradjanin, A.; Masa, J.; Puschhof, A.; Stroka, J.; Kulesza, P. J.; Schuhmann, W. Application of SECM in tracing of hydrogen peroxide at multicomponent non-noble electrocatalyst films for the oxygen reduction reaction. *Catal. Today* **2013**, 202, 55–62.
- (23) Armstrong, D. A.; Huie, R. E.; Koppenol, W. H.; Lymar, S. V.; Merényi, G.; Neta, P.; Ruscic, B.; Stanbury, D. M.; Steenken, S.; Wardman, P. Standard electrode potentials involving radicals in aqueous solution: inorganic radicals (IUPAC Technical Report). 2015, 87 (11–12), 1139–1150.
- (24) Mahne, N.; Renfrew, S. E.; McCloskey, B. D.; Freunberger, S. A. Electrochemical Oxidation of Lithium Carbonate Generates Singlet Oxygen. *Angew. Chem., Int. Ed.* **2018**, *57* (19), 5529–5533.
- (25) Cao, D.; Tan, C.; Chen, Y. Oxidative decomposition mechanisms of lithium carbonate on carbon substrates in lithium battery chemistries. *Nat. Commun.* **2022**, *13* (1), 4908.
- (26) Sarbapalli, D.; Mishra, A.; Rodríguez-López, J. Pt/Polypyrrole Quasi-References Revisited: Robustness and Application in Electrochemical Energy Storage Research. *Anal. Chem.* **2021**, *93* (42), 14048–14052.
- (27) Houchins, G.; Pande, V.; Viswanathan, V. Mechanism for Singlet Oxygen Production in Li-Ion and Metal—Air Batteries. *ACS Energy Lett.* **2020**, 5 (6), 1893—1899.
- (28) Nioradze, N.; Chen, R.; Kim, J.; Shen, M.; Santhosh, P.; Amemiya, S. Origins of Nanoscale Damage to Glass-Sealed Platinum Electrodes with Submicrometer and Nanometer Size. *Anal. Chem.* **2013**, 85 (13), 6198–6202.
- (29) Henstridge, M. C.; Compton, R. G. Mass Transport to microand nanoelectrodes and their arrays: a review. *Chem. Rec.* **2012**, *12* (1), 63–71.
- (30) Kai, T.; Zhou, M.; Duan, Z.; Henkelman, G. A.; Bard, A. J. Detection of CO₂• in the Electrochemical Reduction of Carbon Dioxide in N,N-Dimethylformamide by Scanning Electrochemical Microscopy. *J. Am. Chem. Soc.* **2017**, 139 (51), 18552–18557.
- (31) Zhou, M.; Yu, Y.; Hu, K.; Mirkin, M. V. Nanoelectrochemical Approach To Detecting Short-Lived Intermediates of Electrocatalytic Oxygen Reduction. *J. Am. Chem. Soc.* **2015**, *137* (20), 6517–6523.
- (32) Lefrou, C.; Cornut, R. Analytical Expressions for Quantitative Scanning Electrochemical Microscopy (SECM). *ChemPhysChem* **2010**, *11* (3), 547–556.
- (33) Laoire, C. O.; Mukerjee, S.; Abraham, K. M.; Plichta, E. J.; Hendrickson, M. A. Elucidating the Mechanism of Oxygen Reduction for Lithium-Air Battery Applications. *J. Phys. Chem. C* **2009**, *113* (46), 20127–20134.
- (34) Laoire, C. O.; Mukerjee, S.; Abraham, K. M.; Plichta, E. J.; Hendrickson, M. A. Influence of Nonaqueous Solvents on the Electrochemistry of Oxygen in the Rechargeable Lithium—Air Battery. *J. Phys. Chem. C* **2010**, *114* (19), 9178—9186.